

MODELING AND CONTROL OF THIN MEMBRANE STRIPS

Eric J. Ruggiero and Daniel J. Inman

Center for Intelligent Material Systems and Structures
Virginia Polytechnic Institute and State University
Blacksburg, VA 24061-0261, USA

Abstract

Ultra-lightweight, ultra-large and deployable satellite technology is at the forefront of research efforts for future on-orbit reconnaissance missions. The minimal mass and stowage volume associated with the technology are attractive traits for getting larger bandwidth satellites on-orbit. One of the key components for such a satellite is the membrane lens or aperture for optical or radar applications, and understanding the membrane's dynamics is critical for mission success. As either an optical reflector or radar antenna, the vibration levels of the membrane must be minimized and eliminated. This work examines the possibility of integrating a PZT bimorph near the boundary of a strip sample to eliminate detrimental vibration. By starting with a 1-D model, the dominant governing phenomena of the system dynamics can be established and used to build more complex models with confidence.

A physics-based finite element (FE) model of a thin strip of Kapton HN material with a monolithic PZT bimorph bonded near a boundary is developed in a MatLab environment and verified experimentally. The membrane strip under tension is modeled as a beam under axial load. In doing so, the FE model is able to capture the relevant transverse dynamics of the experimental setup. Having verified the FE model, an LQR controller is developed and simulated to demonstrate effective control over the transverse dynamics of the membrane sample. In addition, insight into the optimal placement of sensors is garnered through the careful mathematical development of the distributed parameter problem.

Introduction

In order to increase satellite imaging and communication capabilities from on-orbit, satellite

apertures will require larger operating areas. Getting larger space optics or communication arrays on-orbit translates into ultra-flexible aperture designs that demonstrate both packaging efficiency and deployment reliability. However, such craft also pose challenging structural vibration and control issues (Huang, 1994; Gibson and Adamian, 1991).

Perhaps the most interesting as well as most challenging aspect of future ultra-large, deployable satellites is the membrane optic or communication array itself. For optical imaging purposes, or for that matter, imaging purposes in general, the membrane mirror will need to be held at nanometer tolerances for extended periods of time. Currently, membrane mirror fabrication technology is able to build 1 m apertures with 30 nm peak-to-peak error. Just as impressively, these polymer membranes are cured with an acquired surface roughness of 1 – 2 nm. With material technology solidifying in the area of membrane optic fabrication, the concept of ultra-large membrane mirrors is quickly coming to fruition.

With the development of optical quality membrane mirrors, structural control engineering needs to keep pace with both modeling the rich dynamics of ultra-thin, ultra-flexible membranes as well as in developing suitable controllers for future satellite mission requirements. A desired capability of an ultra large membrane mirror is to be able to mitigate any sort of dynamic disturbance to keep the aperture in focus.

Before attacking the more complex 2-D physics of a membrane lens, we will look at modeling and controlling the dynamics of a 1-D membrane strip with an augmented piezoelectric (PZT) bimorph actuator. The goals of this work are to 1) properly model the physics of the membrane – PZT augmented system and 2) to demonstrate that the PZT bimorph can be used for effective control of the membrane. To account for the

additional mass and stiffness of the actuator, we will assume that the system behaves like a beam under axial loading. Experimental analysis will verify this assumption.

Other researchers have also made efforts in this area of research. Banks and Inman (1991) identified that modal control of a beam structure was insufficient and highlighted the benefits of using the finite element method for system identification and control. Hall, Glaese, and Flint (2002) performed experiments to identify the key structural dynamics of membrane strips, and then used 2-D beam elements to create a model to match the response of the structure. They did not include any piezoelectric material in their model. Rogers and Agnes (2002) used a finite element approach based on the *Method of Integral Multiple Scales* to analyze an axisymmetric, piezothermoelastic laminated plate model representing an active optic element. The results of the research presented show that a piezoelectric polymer adhered to the nonreflective surface of an inflatable optical reflector can have a significant effect on the wavefront being measured. Further, the laminate also could be used as an active vibration suppression element.

Formulation of the Weak Form for a Beam Under Axial Loading

Given the transverse vibration dynamical equation of a beam under axial loading, namely,

$$\frac{\partial^2}{\partial x^2} \left[E(x)I(x) \frac{\partial^2 w(x,t)}{\partial x^2} \right] + \frac{\partial}{\partial x} \left[P(x) \frac{\partial w(x,t)}{\partial x} \right] \dots + \rho(x)A(x) \frac{\partial^2 w(x,t)}{\partial t^2} = 0 \quad (1)$$

we wish to derive the weak form of these dynamics for the purpose of applying finite elements to create a system model. In Equation 1, the sign convention of $P(x)$ is positive if the applied axial load is compressive and negative if the applied axial load is tensile. Notice that we have let the axial load be a function of x , meaning the applied load does not have to be uniform throughout the beam. Further, $E(x)$ is the elastic modulus, $I(x)$ is the area moment of inertia, $\rho(x)$ is the density, and $A(x)$ is the cross-sectional area of the beam.

First, we assume that the system consists of two states, position and velocity, or $w(x,t)$ and $v(x,t)$, respectively. Then we can write two equations,

$$w_t(x,t) = v(x,t) \quad (2a)$$

$$\rho(x)A(x)v_t(x,t) = - \left[E(x)I(x)w_{xx}(x,t) \right]_{xx} - \left[P(x)w_x(x,t) \right]_x \quad (2b)$$

Now we will multiply through both Equations 2a and 2b by test functions $\phi(x)$ and $\psi(x)$, respectively, and then integrate the equations over the span of the structure. Doing so yields the equations:

$$\frac{\partial}{\partial t} \int_0^L w(x,t)\phi(x) dx = \int_0^L v(x,t)\phi(x) dx \quad (3a)$$

$$\frac{\partial}{\partial t} \int_0^L \rho(x)A(x)v(x,t)\psi(x) dx = - \int_0^L \left[E(x)I(x)w_{xx}(x,t) \right]_{xx} \psi(x) dx \dots - \int_0^L \left[P(x)w_x(x,t) \right]_x \psi(x) dx \quad (3b)$$

Next, we integrate Equation 3b by parts. Doing so yields:

$$\frac{\partial}{\partial t} \int_0^L \rho(x)A(x)v(x,t)\psi(x) dx = - \int_0^L \left[E(x)I(x)w_{xx}(x,t) \right] \psi_{xx}(x) dx \dots + \int_0^L \left[P(x)w_x(x,t) \right] \psi_x(x) dx + \left[E(x)I(x)w_{xx}(x,t)\psi_x(x) \right]_0^L \dots - \left[E(x)I(x)w_{xx}(x,t) \right]_x \psi(x) \Big|_0^L - \left[P(x)w_x(x,t) \right] \psi(x) \Big|_0^L \quad (4)$$

For the system we are trying to model, we will assume that the boundary conditions are pinned-pinned. A pinned end cannot translate in any direction and also cannot sustain a bending moment. Mathematically speaking, these conditions are imposed through the following boundary conditions:

$$w(0,t) = w(L,t) = 0 \quad (5a)$$

$$E(0)I(0)w_{xx}(0,t) = E(L)I(L)w_{xx}(L,t) = 0 \quad (5b)$$

Now, we wish to enforce the boundary conditions, Equations 5, in Equation 4. Notice that the first boundary term of Equation 4 vanishes because of the natural boundary conditions imposed by Equation 5b, and, by forcing

$$\psi(0) = \psi(L) = 0, \quad (6)$$

the second and third boundary terms in Equation 4 also vanish. Hence, we arrive at the weak form of Equation 4, given by

$$\begin{aligned}
& \frac{\partial}{\partial t} \int_0^L \rho(x) A(x) v(x, t) \psi(x) dx = \dots \\
& - \int_0^L [E(x) I(x) w_{xx}(x, t)] \psi_{xx}(x) dx \dots \quad (7) \\
& + \int_0^L [P(x) w_x(x, t)] \psi_x(x) dx
\end{aligned}$$

Next, we wish to approximate the dynamics given by Equations 3a and 7. To do so, we let

$$\begin{aligned}
w(x, t) &= \sum_{i=1}^N w_i(t) \phi_i(x) \\
v(x, t) &= \sum_{i=1}^N v_i(t) \phi_i(x)
\end{aligned} \quad (8)$$

Note that the test functions introduced in Equations 3 were dummy functions yet to be determined, and therefore, since they live in the same Hilbert space, $H^2(0, L) \cap H_0^1(0, L)$, we can let $\varphi(x) = \psi(x)$. Plugging in our approximations (Equations 8) into Equations 3a and 7 yields:

$$\frac{\partial}{\partial t} \sum_{i=1}^N w_i \int_0^L \phi_i \phi_j dx = \sum_{i=1}^N v_i \int_0^L \phi_i \phi_j dx \quad (9a)$$

$$\frac{\partial}{\partial t} \sum_{i=1}^N v_i \int_0^L \rho A \phi_i \phi_j dx = \sum_{i=1}^N w_i \int_0^L P(\phi_i)_x (\phi_j)_x dx \dots \quad (9b)$$

$$- \sum_{i=1}^N w_i \int_0^L EI(\phi_i)_{xx} (\phi_j)_{xx} dx$$

By letting

$$\begin{aligned}
M_1 &= \left[\int_0^L \phi_i \phi_j dx \right]_{i,j=1}^N \\
M_2 &= \left[\int_0^L \rho A \phi_i \phi_j dx \right]_{i,j=1}^N \\
A_{11} &= \left[\int_0^L P(\phi_i)_x (\phi_j)_x dx \right]_{i,j=1}^N \\
A_{22} &= \left[\int_0^L EI(\phi_i)_{xx} (\phi_j)_{xx} dx \right]_{i,j=1}^N
\end{aligned} \quad (10)$$

we arrive at the finite element matrix form of the dynamic equations governing the transverse vibration of the system,

$$\begin{bmatrix} M_1 & 0 \\ 0 & M_2 \end{bmatrix} \begin{bmatrix} \bar{w} \\ \bar{v} \end{bmatrix}_t = \begin{bmatrix} 0 & M_1 \\ [A_{11} - A_{22}] & 0 \end{bmatrix} \begin{bmatrix} \bar{w} \\ \bar{v} \end{bmatrix}. \quad (11)$$

Addition of Viscous Air Damping and Kelvin-Voigt Damping

Next, we would like to add terms to represent damping imposed by an external fluid medium (like air) and as well as internal damping. To do this, we augment the system dynamics in Equation 1:

$$\begin{aligned}
& \frac{\partial^2}{\partial x^2} \left[E(x) I(x) \frac{\partial^2 w(x, t)}{\partial x^2} \right] + \frac{\partial}{\partial x} \left[P(x) \frac{\partial w(x, t)}{\partial x} \right] \dots \\
& + \rho(x) A(x) \frac{\partial^2 w(x, t)}{\partial t^2} + \gamma \frac{\partial w(x, t)}{\partial t} \dots \quad (12) \\
& + \frac{\partial^2}{\partial x^2} \left[\beta(x) I(x) \frac{\partial^3 w(x, t)}{\partial x^2 \partial t} \right] = 0
\end{aligned}$$

The constant term γ is based on the external fluid medium, whereas the term $\beta(x)$ represents the energy dissipation by friction internal to the beam. Now we will focus on Equation 12, as Equations 2a, 3a and 9a do not change through the introduction of the damping terms. Following the same procedure as previously outlined, we have:

$$\begin{aligned}
\rho(x) A(x) v_t(x, t) &= -[E(x) I(x) w_{xx}(x, t)]_{xx} \dots \\
& - [P(x) w_x(x, t)]_x - \gamma v(x, t) - [\beta(x) I(x) v_{xx}(x, t)]_{xx}
\end{aligned} \quad (13)$$

Multiplying through by our test functions and integrating yields:

$$\begin{aligned}
& \frac{\partial}{\partial t} \int_0^L \rho(x) A(x) v(x, t) \psi(x) dx = - \int_0^L [E(x) I(x) w_{xx}(x, t)] \psi_{xx}(x) dx \dots \\
& + \int_0^L [P(x) w_x(x, t)] \psi_x(x) dx + [E(x) I(x) w_{xx}(x, t) \psi_x(x)]_0^L \dots \\
& - [E(x) I(x) w_{xx}(x, t)]_x \psi(x) \Big|_0^L - [P(x) w_x(x, t)] \psi(x) \Big|_0^L \dots \\
& - [\beta(x) I(x) v_{xx}(x, t)]_x \psi(x) \Big|_0^L + [\beta(x) I(x) v_{xx}(x, t)] \psi_x(x) \Big|_0^L \dots \\
& - \int_0^L [\beta(x) I(x) v_{xx}(x, t)] \psi_{xx}(x) dx - \gamma \int_0^L v(x, t) \psi(x) dx
\end{aligned} \quad (14)$$

Again, we enforce the boundary conditions from the pinned-pinned beam geometry and set

$$\psi(0) = \psi(L) = 0 \quad (15)$$

Doing so yields the weak form of Equation 13:

$$\begin{aligned}
& \frac{\partial}{\partial t} \int_0^L \rho(x) A(x) v(x, t) \psi(x) dx = \\
& - \int_0^L [E(x) I(x) w_{xx}(x, t)] \psi_{xx}(x) + [P(x) w_x(x, t)] \psi_x(x) dx \dots \\
& - \int_0^L [\beta(x) I(x) v_{xx}(x, t)] \psi_{xx}(x) dx - \gamma \int_0^L v(x, t) \psi(x) dx
\end{aligned} \tag{16}$$

Plugging in our approximations (Equations 8), and by letting:

$$K_1 = \left[\int_0^L \beta I (\psi_i)_{xx} (\psi_j)_{xx} dx \right]_{i,j=1}^N, \tag{17}$$

we can write our approximate system dynamics in matrix form, namely:

$$\begin{bmatrix} M_1 & 0 \\ 0 & M_2 \end{bmatrix} \begin{bmatrix} \bar{w} \\ \bar{v} \end{bmatrix}_t = \begin{bmatrix} 0 & M_1 \\ [A_{11} - A_{22}] & -\gamma M_1 - K_1 \end{bmatrix} \begin{bmatrix} \bar{w} \\ \bar{v} \end{bmatrix}. \tag{18}$$

Finally, we need to construct an input vector that allows the PZT bimorph to exert a distributed moment on the membrane in the form of an induced strain along the beam's surface. Although such a moment term is not differentiable (due to its discontinuity along the membrane's surface), this is of no concern since it is integrated by parts twice to arrive at the weak form. Now, our dynamic equation becomes

$$\begin{bmatrix} M_1 & 0 \\ 0 & M_2 \end{bmatrix} \begin{bmatrix} \bar{w} \\ \bar{v} \end{bmatrix}_t = \begin{bmatrix} 0 & M_1 \\ [A_{11} - A_{22}] & -\gamma M_1 - K_1 \end{bmatrix} \begin{bmatrix} \bar{w} \\ \bar{v} \end{bmatrix} + Bu \tag{19}$$

where

$$B = \begin{bmatrix} 0 \\ M_2^{-1} \bar{b} \end{bmatrix}, \tag{20}$$

and where, after integrating by parts twice,

$$\bar{b} = \int_0^L b(x) \phi_j''(x) dx. \tag{21}$$

Throughout our finite element formulation, we will use the cubic B-splines in both our approximation and as our test functions (Prenter, 1975).

Hardware and Test Stand

The experimental setup consists of a 21.8 x 1.9 cm strip sample of Kapton HN (51 μm thick). Two wafers of H4 piezoelectric material were glued to the membrane sample to serve as the excitation actuator for the system. Copper tape was used as the conductive layer on one side of the H4 PZT wafer to attach one lead wire, and a second lead wire was attached to the opposite side of the PZT wafer using SuperSafe Superior #30 Soft Solder Flux Liquid. A diagram of the membrane sample with attached PZT is shown below in Figure 1. Table 1 describes the relevant material properties of the Kapton (www.dupont.com) and H4 PZT wafer (www.piezo.com).

The Kapton HN sample was held in place by two grippers. Each gripper has two aluminum rods pushed through two opposing channels and are held in place by an interference fit. The rods serve as the contact points to hold the sample in place, and thus form pinned-pinned boundary conditions. The grippers are aligned by bolting them to a frame made of extruded aluminum stock (80/20 series 1515). While one gripper is held permanently in place, the other gripper is attached to a lead screw for easy travel in the x -direction along the axis of the membrane sample. This allows for accurate tensile loads to be applied to the sample. The tensile load applied to the membrane sample is measured by a Transducer Techniques load cell (model #MLP-75). The load cell output is measured by an Omegadyne strain gage meter (model #LC101-50). A picture of the experimental setup, including the H4 PZT bimorph, grippers, and load cell, is shown in Figure 2.

The entire experimental setup was housed in an environmental chamber (Tenney Environmental #27429). While testing in ambient conditions, the chamber served as an excellent shield from external vibratory disturbances, such as air conditioning currents. The response of the membrane sample was measured using a Polytech laser vibrometer (laser head #OFV 303 and control signal box #OFV 3001). The laser vibrometer shines a laser onto the sample and measures either the displacement or velocity (depending on which output channel is selected) of the structure at that particular point through interferometry. The laser vibrometer was selected as the sensor for measuring the response of the system as the mass loading effect from a more traditional accelerometer would have been significant considering the ultra-thin nature of the Kapton sample. A photo of the test setup, including the test chamber and laser vibrometer, is shown in Figure 3. Figure 4 presents a schematic of the entire testing setup, including necessary signal conditioning electronics.

Data Acquisition

The goal of the current work is to identify the transverse vibrations of the membrane sample as a means for comparison to the developed finite element model using the weak form derived previously. The dynamic response of the membrane sample held under tension was tested under ambient conditions. The excitation to the structure was provided by the PZT bimorph. Under such excitation, the PZT bimorph will generate a distributed moment to the sample, thus exciting the out-of-plane, or transverse, vibrations.

The excitation signal was generated via MatLab's SigLab Data Acquisition board. SigLab interfaces through a SCSI card with a PC system and provides a relatively inexpensive means for performing dynamic system analysis. Using SigLab's VNA and VFG toolkits, a burst chirp signal with a peak amplitude of 0.5 V and with frequency content ranging from 0.1 –

325 Hz was generated to excite the PZT bimorph. The burst chirp signal was amplified by a factor of 50 through a Trek Amplifier (model 50/750). The velocity response of the structure was measured using the laser vibrometer at twenty equally spaced points (approximately) along the centerline of the membrane strip, one point at a time. The velocity signal was fed into an Ithaco Filter with the low-pass cut-off frequency set to 350 Hz to eliminate any high-frequency noise from the response. The filtered velocity signal was then fed back to input Channel 2 on the SigLab DAQ board. Transfer functions were measured at each of the twenty centerline points along the length of the Kapton sample. Each point was designated with a small, square piece of highly-reflective tape to help eliminate detrimental backscatter from the laser, consequently improving the quality of the measured signal.

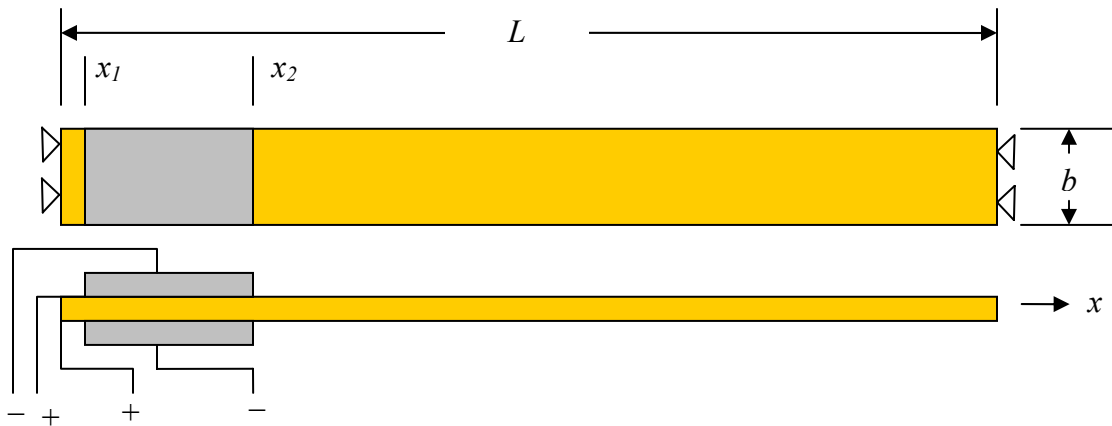


Figure 1. Diagram of the Kapton HN sample with attached PZT bimorph, including top view (above) and side view (below).

Table 1. Relevant material properties for Kapton HN and H4 PZT.

	Parameter	Symbol	Value
Kapton HN	modulus	E	230 MPa
	length	L	21.8 cm
	width	b	1.9 cm
	thickness	t	51 μm
	density	ρ	1400 kg/m^3
	viscous air damping	γ	0.02
	Poisson's ratio	ν	0.34
	shear modulus	G	86.2 MPa
H4 PZT Wafer	coupling coefficient	d_{31}	4.2 pm/V
	modulus	E_{pzt}	2.86 GPa
	patch length	L_{pzt}	3.8 cm
	patch width	b_{pzt}	1.9 cm
	patch thickness	t_{pzt}	533.4 μm
	density	ρ_{pzt}	5300 kg/m^3
	Poisson's ratio	ν_{pzt}	0.31
	shear modulus	G_{pzt}	2.36 GPa

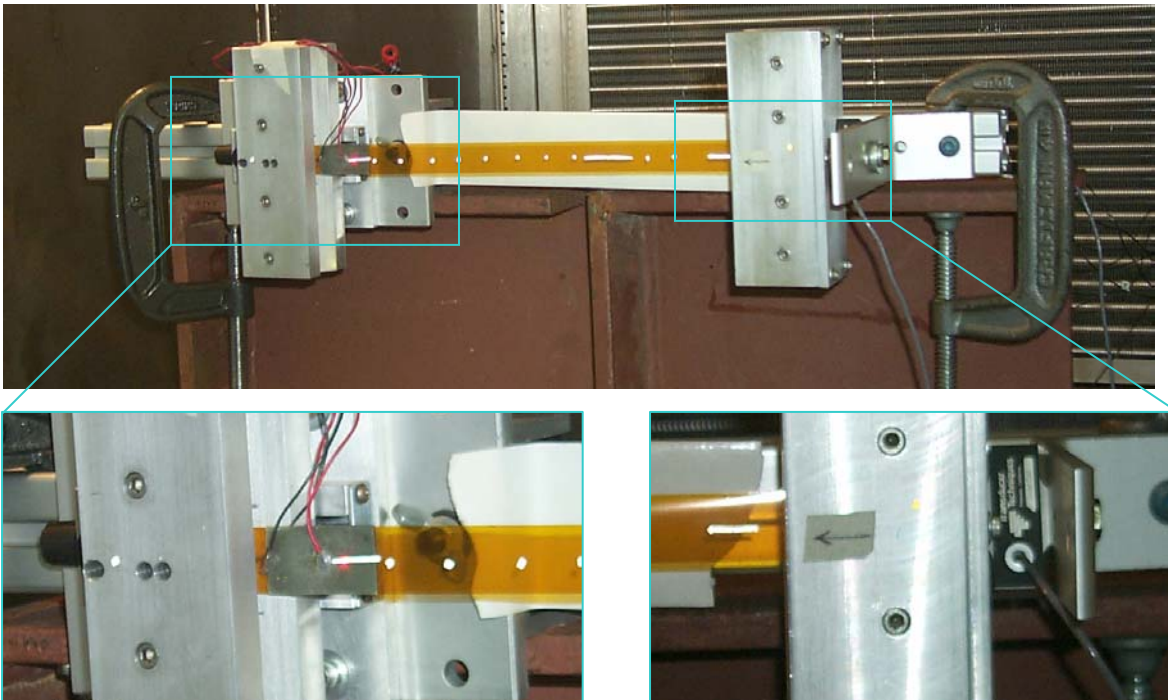


Figure 2. Photograph of the experimental setup showing the Kapton membrane held under tension (top), with close-up photos of the PZT bimorph (bottom left) and Transducer Techniques load cell (bottom right). In this picture, the left gripper is attached to the lead screw.



Figure 3. Photograph of the test setup, highlighting the laser vibrometer sensor and the Kapton sample test rig sitting inside of the Tenney Environmental chamber.

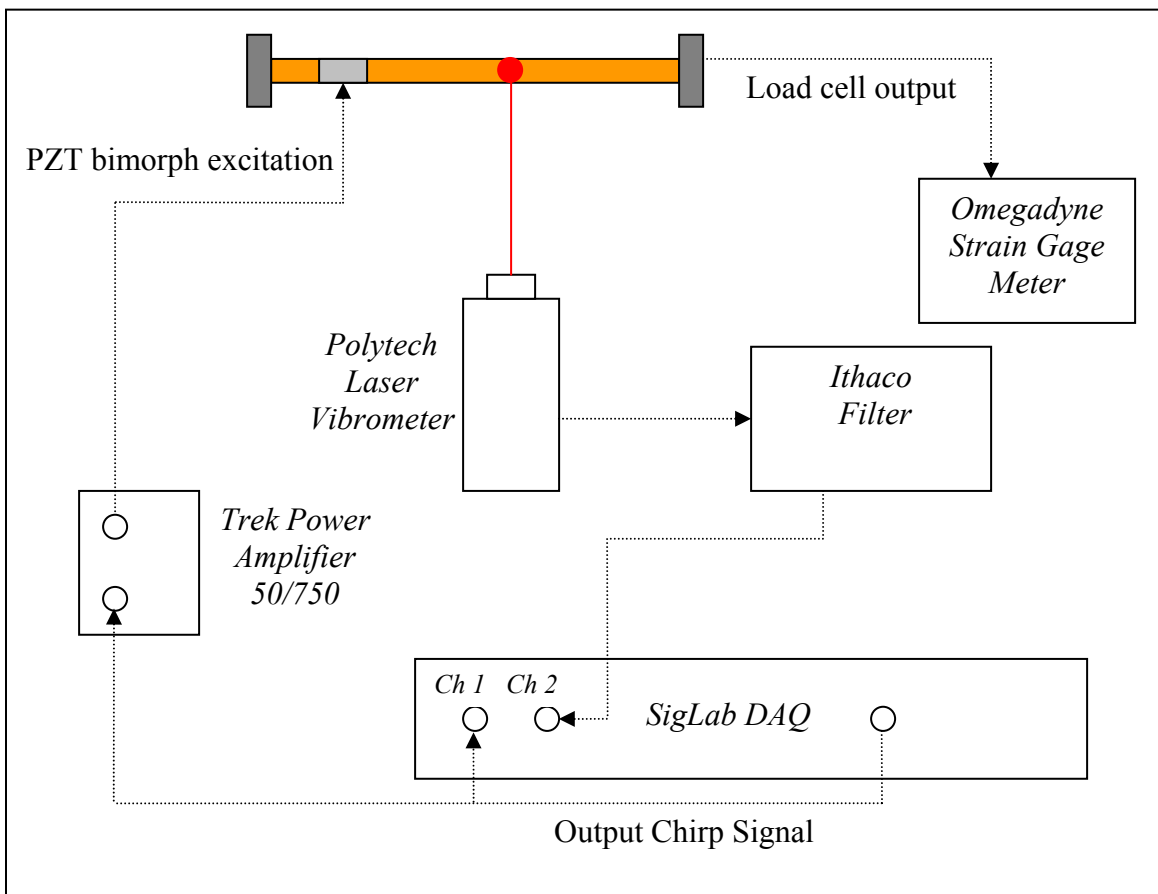


Figure 4. Schematic of the experimental testing setup to capture the dynamic response of the Kapton sample.

Experimental Results

Figure 5 shows the collected frequency response functions of the test sample plotted on the same axes. The key dynamics in the frequency range of 0 – 325 Hz occur at the peaks within the frequency response functions, or more specifically, at 73.0, 214.4, and 282.0 Hz. The sample was held in tension at 10.5 N.

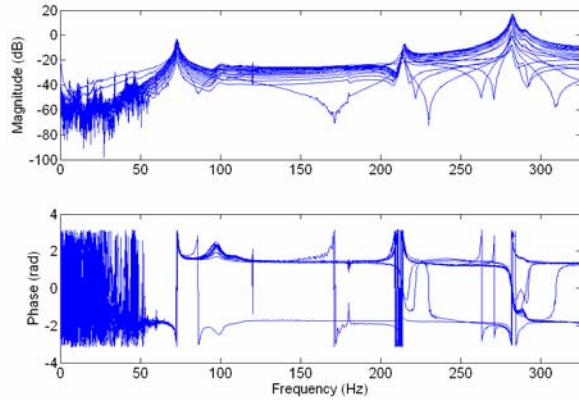


Figure 5. Bode plots of the membrane – PZT system taken at 20 locations along the length of the sample.

Now that we have experimental data, we now want to compare the collected data to our developed FE model.

Comparison Between FE Model and Experimental Results

The next step in our analysis is to see how well our developed FE model compares to the actual experimental data. Figure 6 compares the predicted response of the system at a point measured 8.4 cm from the left-hand boundary. The FE model was shown to converge with 256 elements.

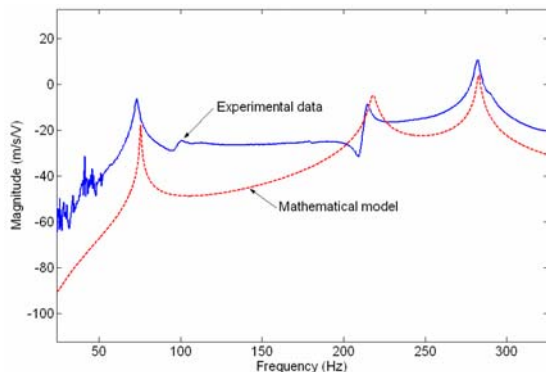


Figure 6. Frequency response comparison between FE model and experimental data at $x = 8.4$ cm.

As seen in Figure 6, the FE model does an excellent job of identifying the key structural frequencies of the system. It predicts the first three

resonant frequencies to within 3%. Even though the predicted response curve does not lie exactly on top of the experimental data, similar dynamic trends are observed between the two curves. Another good point of comparison between the FE model and the experimental data is the correlation between the predicted and actual mode shapes of the structure. Mode shapes are the structure's shape of vibration at particular frequencies. Figures 7 and 8 compare the predicted and actual mode shapes of the membrane-PZT system.

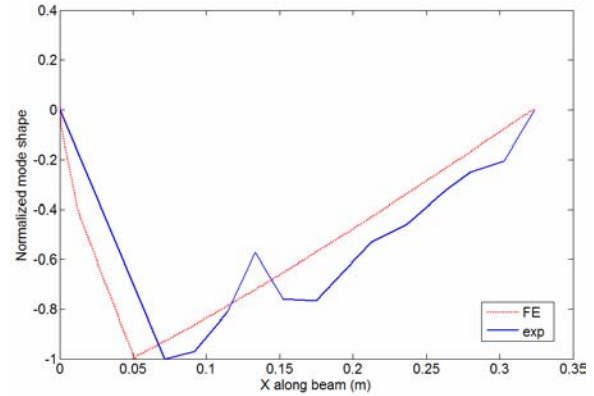


Figure 7. Mode shape comparison between the FE model and experimental data.

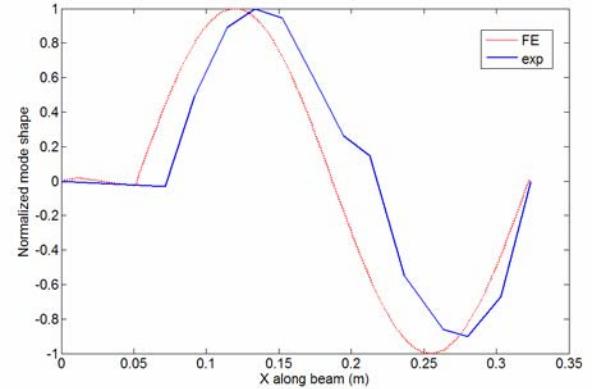


Figure 8. Mode shape comparison between the FE model and experimental data.

The excellent agreement between the predicted and actual response of the structure from both a frequency domain perspective and from a mode shape perspective provides strong support in validating the proposed FE model.

Next, the ability of the FE model to predict the response of the structure at different loadings was also tested. A summary of the predicted resonant frequencies and measured resonant frequencies at loadings of 6.9, 8.8, and 12.0 N is summarized in Table 2.

Table 2. Comparison of predicted and actual frequencies of the test sample at different tensile loadings.

Tension (N)	Exp ω_1 (Hz)	Model ω_1 (Hz)	% Error
6.9	62	62	0.3
8.8	68	70	-2.5
12.0	77	82	-6.5
Tension (N)	Exp ω_2 (Hz)	Model ω_2 (Hz)	% Error
6.9	175	178	-2.0
8.8	196	201	-2.5
12.0	226	234	-3.5
Tension (N)	Exp ω_3 (Hz)	Model ω_3 (Hz)	% Error
6.9	225	231	-2.8
8.8	258	261	-1.0
12.0	300	304	-1.3

As shown by the minimal errors given in Table 2, the FE model does an excellent job of predicting the frequency response of the membrane sample with attached PZT bimorph up to 325 Hz for a variety of load cases. Now that we have a well-developed model, the next goal is to use the PZT bimorph to apply control to our structure for dynamic disturbance rejection.

LQR Control of the Membrane Strip

Now, we wish to construct an LQR controller to use the PZT bimorph as an actuator to eliminate detrimental vibration to the Kapton strip. The optimal control problem is stated as follows:

Given $z(0) \in R^{2N}$, a vector containing the states of the system, choose a control $u \in L_2(0, \infty; R^m)$ to minimize the cost functional

$$J_N(z(0), u) = \int_0^\infty [z(t)^T Q^N z(t) + u(t)^T R u(t)] dt. \quad (22)$$

Q^N is a symmetric, non-negative $2n \times 2n$ matrix, and R is a scalar value since we only have one control input (the voltage supplied to the PZT bimorph actuator). We can define our Q^N matrix in the following manner. Following the methodology of Gibson and Adamian (1991), we will define the entries to the Q^N matrix based on the kinetic and potential energies of the system. We can thereby define

$$Q^N = \begin{bmatrix} Q_1^N & 0 \\ 0 & Q_2^N \end{bmatrix} \quad (23)$$

where

$$Q_1^N = q_1 \int_0^L \{A_{11} - A_{22}\} dx \quad (24)$$

and

$$Q_2^N = q_2 \int_0^L \{\rho A(\psi_i)(\psi_j)\} dx. \quad (25)$$

The terms q_1 and q_2 are weighting terms that can be determined by the control designer. For completeness, the R matrix for this particular LQR problem is defined as

$$R = [r]. \quad (26)$$

The upper and lower diagonal entries of the Q^N matrix correspond to twice the total energy of the structure (Gibson and Amadian, 2001). The optimal control, u_N , is given by

$$u_N = -K^N z(t), \quad (27)$$

where

$$K^N = R^{-1} [B^N]^T \Pi^N \quad (28)$$

and Π^N is the minimal, symmetric, non-negative solution to the Riccati equation

$$[A^N]^T \Pi^N + \Pi^N A^N - \Pi^N B^N R^{-1} [B^N]^T \Pi^N + Q^N = 0 \quad (26)$$

Implementing this control design with our Kapton—PZT bimorph structure, and choosing

$$[q_1 \quad q_2 \quad r] = [100 \quad 1 \quad 0.01], \quad (29)$$

we can now compare the uncontrolled and controlled response of the membrane subject to initial disturbance modeled as the displacement

$$w(0) = \frac{1}{256} \sin\left(\frac{3\pi}{L} x\right). \quad (30)$$

Figures 9 and 10 show the uncontrolled and controlled response of the structure, respectively.

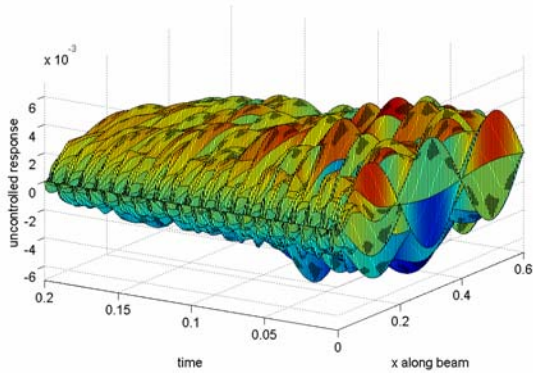


Figure 9. Uncontrolled response of the membrane.

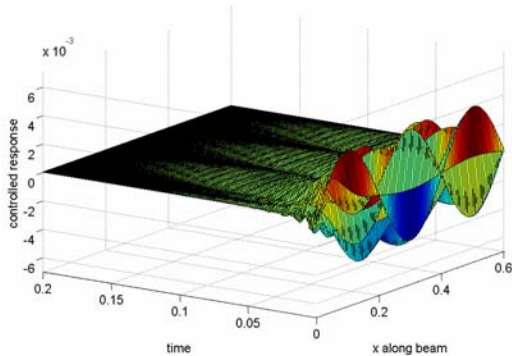


Figure 10. Controlled response of the membrane.

As shown in Figure 10, the response of the membrane is effectively damped out and eliminated after 0.15s. Consequently, the membrane optic or radar could be brought back into focus in a short amount of time. The LQR controller can be tailored such that the response of the system is damped out in a faster manner; however, the tradeoff would be a greater amount of control effort required by the bimorph. For these settings, the bimorph required a peak voltage of 40V.

Summary of Results

A 1-D finite element model of a Kapton membrane strip augmented with a PZT bimorph has been developed and verified experimentally. The FE model needed to use beam theory and treat the system as a beam under axial load in order to account for the added mass and stiffness of the PZT bimorph. The model can accurately predict the response of the structure up to 325 Hz, capturing the first three resonant frequencies of the system. Further, the model has been validated for tensions varying between 6.9 and 12.0 N. An LQR controller has been developed and through simulation has demonstrated that the response of the membrane can be highly damped through the applied control of the PZT bimorph. This research has laid the foundation for

future work in the area of ultra-lightweight space optics with integrated smart materials.

Acknowledgements

The authors wish to thank the National Science Foundation and Virginia Space Grant Consortium for funding this research. Also, the contributions of both the Air Force Research Lab (AFRL) and Air Force Office of Scientific Research (AFOSR) are gratefully acknowledged.

References

Banks, H.T. and D.J. Inman. "On Damping Mechanisms in Beams," *Journal of Applied Mechanics – Transactions of the ASME*, 58 (3), 716 – 723, September 1991.

Gibson, J.S. and A. Adamian. "A Comparison of Three Approximation Schemes for Optimal Control of a Flexible Structure." *SIAM Journal of Control and Optimization*, V 29, No. 1, pp. 1-37, 1991.

Hall, J., R. Glaese, and E. Flint. "Dynamic Behavior of Thin Film Membrane Strips," AIAA Paper #2002-1378, 2002.

Huang, Wei. *Compensator Design for a System of Two Connected Beams*. Doctor of Philosophy in Mathematics Dissertation, Virginia Polytechnic Institute and State University, 1994.

Prenter, P.M. *Splines and Variational Methods*. John Wiley and Sons (New York), 1975.

Rogers, C. and Agnes, G. S., "Active Axisymmetric Optical Membranes," AIAA Paper 2002-1450, April 2002.

"Properties of Kapton HN Films," www.dupont.com.

"Properties of H4 Piezo Sheets," www.piezo.com.